

# Ultrafast Mapping of Coherent Dynamics and Density Matrix Reconstruction in Terahertz-Assisted Laser Field

Yizhu Zhang,<sup>1,2</sup> Tian-Min Yan,<sup>1,\*</sup> and Y. H. Jiang<sup>1,3,4,†</sup>

<sup>1</sup>*Shanghai Advanced Research Institute,*

*Chinese Academy of Sciences, Shanghai 201210, China*

<sup>2</sup>*Center for Terahertz waves and College of Precision*

*Instrument and Optoelectronics Engineering,*

*Key Laboratory of Opto-electronics Information and Technical Science,*

*Ministry of Education, Tianjin University, China*

<sup>3</sup>*University of Chinese Academy of Sciences, Beijing 100049, China*

<sup>4</sup>*ShanghaiTech University, Shanghai 201210, China*

## Abstract

A time-resolved spectroscopic protocol exploiting terahertz-assisted photoionization is proposed to reconstruct transient density matrix. Population and coherence elements are effectively mapped onto spectrally separated peaks in photoionization spectra. The beatings of coherence dynamics can be temporally resolved beyond the pulse duration, and the relative phase between involved states is directly readable from the oscillatory spectral distribution. As demonstrated by a photo-excited multilevel open quantum system, the method shows potential applications for sub-femtosecond time-resolved measurements of coherent dynamics with free electron lasers and tabletop laser fields.

Quantum coherence derived from the principle of superposition is a fundamental concept in quantum mechanics and a ubiquitous phenomenon with the time scale ranging from milliseconds, as in delicately prepared cold atoms, to attoseconds for electronic coherence in field-perturbed atoms [1] and molecules [2]. Although the coherence dynamics take a key role in photo-reactions [3–5], the real-time observation of electronic coherence is highly challenging, particularly on the femtosecond or even attosecond timescale. In photo-ionization processes in atoms and molecules, the electronic coherence prepared by shaking the inner-shell electrons has been uncovered to lose within  $\sim 1$  fs. The decoherence is closely related to the correlation between the photoelectron and the parent ion, significantly affecting the formation of coherent hole wave packets [1, 2]. In addition, for the recently investigated photosynthetic complexes, the possible mechanism of coherence-assisted energy transfer is explored by the multi-dimensional optical spectroscopy [3]. Due to the involvement of multiple transport pathways in the extremely complicated biomolecular environment, further supporting evidences from experimental observations are still required. The observation of ultrafast electronic coherence dynamics is indispensable to provide valuable insight into these fundamental processes. Despite of the significance, ultrafast coherence dynamics are not readily obtained from commonly used time-resolved (pump-probe) spectroscopies, since the comparatively large population signal usually conceals the signature of the coherence.

The complete dynamic information of an open quantum system is encoded in the time-evolved density matrix elements  $\rho_{ij}(\tau)$ , including the population  $\rho_{ii}$  and the coherence  $\rho_{ij}$  ( $i \neq j$ ). The  $\rho_{ij}(\tau)$ -reconstruction from dedicated designed experiments, e.g., the quantum process tomography with the multi-dimensional spectroscopy to fully describe a quantum black box [6], is always desirable. The temporal resolution of optical spectroscopy, however, is temporally restricted to tens of femtoseconds. Since the quantum states are typically prepared and probed by femtosecond-duration pulses, the convolution with the probing pulse leads to the smear of signatures of faster electronic coherences.

In this sense, observing the ultrafast electronic coherence in atoms and molecules, in principle, requires the attosecond metrology. Exploiting the attosecond transient absorption spectroscopy, the electronic coherence of the valence electron in krypton ions was measured with the sub-femtosecond temporal accuracy [7]. The same spectroscopic methodology also allows observing the correlated two-electron coherence motion in helium with attosecond temporal resolution [8]. Although the attosecond metrology can probe the electron wave-

packet motion with high temporal resolution, it requires tremendous efforts with sophisticated laser techniques, including the precise control of both the amplitude and phase of the femtosecond light field throughout the measurement. Moreover, contributions from population and coherence are overlapped after one-dimensional spectral projections, thus usually concealing quantum coherence. For the recently developed free-electron-laser (FEL) facilities, the compression of the pulse with high energetic photons (from extreme ultraviolet to hard X-ray region) down to the sub-femtosecond scale is difficult, obstructing further insights into ultrafast electronic coherence. Kowalewski *et al.* proposed to record the sub-femtosecond electronic coherence using a femtosecond probe pulse [9]. The photoelectron is driven by a phase-locked near infrared (NIR) pulse and multiple sidebands around the characteristic peaks are created. The sidebands carry the high-resolution information of coherence, yet simultaneously complicate the spectroscopic analysis due to the possibly contaminated characteristic spectral features. Moreover, the prerequisite that the photon energy of the streaking field has to be resonant with the relevant states may become a restriction.

In this work, we propose a spectroscopic method to retrieve the full information of the density matrix, like the two-dimensional spectroscopy, unraveling the contributions of coherence in an extra dimension. Exploiting the femtosecond extreme ultraviolet (XUV) pulse and terahertz (THz) streaking field, we show density matrix elements directly map into the photoelectron spectra. Especially, the method in principle allows observing the motion of the electronic wave packet in FEL facilities. In contrast to proposals operating in the so called "sideband regime" [9], our method works in the "streaking regime" [10]. Moreover, without the restriction that the photon energy must match the energy gap between coherently excited states [9], the method can be applied in systems without *a priori* knowledge. Conventionally, the streaking technique is used to characterize the temporal profile of ultrashort pulses, e.g., the attosecond streaking technique that calibrates an attosecond pulse using a moderately strong NIR light field [11], the FEL calibration using the THz or IR-streaking pulse [10, 12, 13]. Here, instead of field diagnosis, the THz-streaking technique is used to investigate ultrafast dynamics.

For a multilevel open quantum system, the scheme of the streaking-assisted photoionization is illustrated in Fig. 1(a). The probe fields, as proposed in this work, comprise a femtosecond XUV pulse and a well synchronized THz pulse, the zero-crossing of whose vector potential is required to be locked at the center of the XUV pulse. As illustrated

by the inset of Fig. 1(a), the combination of the two pulses realizes a two-step process. First, the single-photon ionization induced by the XUV pulse liberates the electron of the superposed state at  $\tau$ , taking a frozen snapshot of quantum states exactly at that time. The THz wave then drives the photoelectron, kinetically rearranging electronic trajectories and inducing the interference between trajectories from different states in the final momentum distribution  $w(p; \tau)$ , which is a critical step to the observation of the coherence. We will show that, the dynamics of the system at any time  $\tau$  as described by  $\rho_{ij}(\tau)$  [Fig. 1(b)] are mapped directly onto  $w(p; \tau)$ , with different elements differentiated by longitudinal momentum  $p$ . Scanning over  $\tau$ , the measured  $w(p; \tau)$ , as shown in Fig. 1(c) and (d), allows for reconstructing the time evolved  $\rho_{ij}(\tau)$ . Without the THz field [Fig. 1(c)], spectral peaks depict the time-evolved populations, which can also be measured using other time-resolved techniques. With the THz field [Fig. 1(d)], interference fringes are formed upon broadened peaks, which is of essential concern due to the encoded information of coherence. All details of these figures can be referred to Fig. 3. The further analysis shows that  $w(p; \tau)$  is composed of a series of Gaussian peaks corresponding to all  $\rho_{ij}(\tau)$ , laying the foundation for  $\rho_{ij}(\tau)$ -reconstruction. The method provides an alternative tool to investigate the decoherence of attosecond photo-ionization in atoms and molecules, and the coherence energy transport in complex photo-reaction systems.

The  $w(p; \tau)$  to measure in the experiment can be analyzed under the strong field approximation. Assuming the atom is subject to linearly polarized fields,  $E(t) = E_{\text{XUV}}(t) + E_{\text{THz}}(t)$ , the ionization signal  $w(p; \tau) = |p| |M_p(\tau)|^2$  is collected along the polarization direction. Neglecting the high-order above threshold ionization, the amplitude of the direct ionization in the length gauge reads  $M_p(\tau) = \lim_{t \rightarrow \infty} \int_0^t dt' e^{iS_p(t')} \langle p + A(t') | \hat{\mu} E(t') | \Psi_0(t') \rangle$ , where  $A(t) = A_{\text{XUV}}(t) + A_{\text{THz}}(t)$  is the vector potential and  $S_p(t') = \frac{1}{2} \int_0^{t'} dt'' [p + A(t'')]^2$ . Note,  $\tau$  is hidden as the temporal center of pulses in  $A(t)$  and  $E(t)$ .  $\hat{\mu}$  is the transition dipole, and  $|\Psi_0(t)\rangle$  is the initial (superposition) state. The photoelectron emission process consists of two steps. The laser field firstly liberates the electron from the atom when the XUV pulse plays a dominant role. Subsequently, the photoelectron is drifted to the final momentum. Since the amplitudes  $|A_{\text{XUV}}| \ll |A_{\text{THz}}|$ , the free electron is driven dominantly by the THz electric field. According to the analysis of the ionization probability in the streaking regime (see S.I), when amplitudes of the wave functions vary slowly within the temporal window of the XUV pulse, the distribution  $|M_p(\tau)|^2$  comprises Gaussian peaks for all population and

coherence terms,  $|M_p(\tau)|^2 = \frac{\pi(E_0^{(\text{XUV})})^2}{2|b(p)|} [W_{\text{pop}}(p; \tau) + W_{\text{coh}}(p; \tau)]$ , with

$$W_{\text{pop}}(p; \tau) = \sum_i \rho_{ii}(\tau) e^{-\frac{\Omega_{ii}^2(p)}{|b(p)\sigma|^2}}, \quad (1)$$

$$W_{\text{coh}}(p; \tau) = 2 \sum_{i,j < i} \text{Re} \left[ \rho_{ij}(\tau) e^{i \frac{\alpha p \Omega_{ij}(p) \Delta_{ij}}{|b(p)|^2}} \right] \\ \times e^{-\frac{\Omega_{ij}^2(p)}{|b(p)\sigma|^2}} e^{-\frac{(\Delta_{ij}/2)^2}{|b(p)\sigma|^2}}, \quad (2)$$

from which the positions and widths of spectral peaks are easily read. Here,  $\Omega_{ij}(p) = p^2/2 + (I_p^{(i)} + I_p^{(j)})/2 - \omega_{\text{XUV}}$ , where  $\omega_{\text{XUV}}$  is the photon energy of XUV field and  $I_p^{(i)} = -E_i$  is the ionization potential of the  $i$ th state. Spectral peaks appear at  $p$  where  $\Omega_{ij}(p) = 0$ , whose solutions include  $p_{ii} = \pm \sqrt{2(\omega_{\text{XUV}} - I_p^{(i)})}$  for  $\rho_{ii}$ , and  $p_{ij} = \pm \sqrt{2(\omega_{\text{XUV}} - (I_p^{(i)} + I_p^{(j)})/2)}$  that is exactly between  $p_{ii}$  and  $p_{jj}$  for  $\rho_{ij}$  ( $i \neq j$ ). Thus,  $\rho_{ij}(\tau)$  in principle can be inferred from  $w(p_{ij}; \tau)$  at characteristic momentum  $p_{ij}$ . The widths of peaks for both  $W_{\text{pop}}$  and  $W_{\text{coh}}$  are determined by  $|b(p)\sigma| = \sqrt{1/\sigma^2 + (\alpha p \sigma)^2}$  with  $b(p) = 1/\sigma^2 - \alpha p$  dependent on the THz field amplitude  $\alpha$  and the temporal width of XUV field  $\sigma$  (standard deviation). In Eq. (2), though  $W_{\text{coh}}$  is much smaller than  $W_{\text{pop}}$  due to the presence of the last exponential term of  $\Delta_{ij} = I_p^{(i)} - I_p^{(j)}$ , the relative amplitude of  $W_{\text{coh}}$  enhances when the THz field increases. For the energetic spaces spanning over a few eV in typical molecular transitions, the THz electric field of  $\sim \text{kV/cm}$ , which is conveniently provided by tabletop THz sources nowadays, is sufficient to couple the coherently excited states and reveal  $W_{\text{coh}}$ .

In the neighborhood of  $p_{ij}$ , the exponent in the real part of Eq. (2),  $p\Omega_{ij}(p)/|b(p)|^2 \simeq p_{ij}^2(p - p_{ij})/(1/\sigma^4 + \alpha^2 p_{ij}^2)$ , is linearly proportional to  $p$ . Defining  $\varphi_{ij}(\tau) = \Delta_{ij}\tau + \varphi_i - \varphi_j$  the instantaneous relative phase between states  $i$  and  $j$ , whose initial phases are  $\varphi_i$  and  $\varphi_j$ , respectively, the real part in Eq. (2) becomes  $|\rho_{ij}(\tau)| \cos[-\Delta_{ij}\alpha p_{ij}^2(p - p_{ij})/(1/\sigma^4 + \alpha^2 p_{ij}^2) + \varphi_{ij}(\tau)]$ , indicating that the spectral yield oscillates with both  $\tau$  and  $p$ . As expected, the oscillatory frequency  $\Delta_{ij}$  along  $\tau$ -axis agrees with the evolution of  $\rho_{ij}(\tau)$  ( $i \neq j$ ), which can be resolved beyond the duration of the XUV pulse. The oscillation along  $p$ -axis, however, is noteworthy, since it provides a potential single- $\tau$  approach to reconstruct phase  $\varphi_{ij}(\tau)$  without the necessity of scanning over time delay  $\tau$ .

Taking the simplest example of a two-level system, we show the feasibility of coherence imaging and relative phase reconstruction using the THz-streaking method. Assuming the system is prepared in the superposition state with the equal probabilities,  $|\Psi_0(t)\rangle =$

$(|g\rangle e^{-iE_g(t-t_0)+i\varphi_g} + |e\rangle e^{-iE_e(t-t_0)+i\varphi_e})/\sqrt{2}$ , with  $|g\rangle$  and  $|e\rangle$  the ground state and excited state of energies  $E_g$  and  $E_e$ , respectively. Here we consider a system with  $E_g = -13.6$  eV and  $E_e = -3.4$  eV, and initial phases are  $\varphi_e = \varphi_g = 0$  at the initial time  $t_0 = 0$  fs. The photon energy of the XUV pulse is 2 a.u. (54.4 eV) with the peak field amplitude 0.005 a.u. (intensity  $\sim 9 \times 10^{11}$  W/cm<sup>2</sup>), and the duration is 5 fs. The center frequency of the single-cycle THz pulse is 4 THz and the peak field strength is 0.001 a.u. ( $\sim 5$  MV/cm). In principle, the requirement that XUV pulse is temporally locked at the zero-crossing of  $A_{\text{THz}}(t)$  can be satisfied in the FEL facility, where the XUV and THz pulses, generated by the same electron bunch from the linear accelerator, are well synchronized [12]. The jitter between the excitation pulse and probing FEL pulse is hardly controlled within attosecond accuracy nowadays, but the restriction can be overcome by the continuously developed technique of synchronization. Since there is no need for the single- $\tau$  measurement, the reliable statistics of spectra can be provided with state-of-art synchronization of the pulse sequence. In our approach, the Fourier transform limited XUV pulse is required. Although Fourier transformation limited pulse is not conveniently delivered in the self-amplified spontaneous emission (SASE) mode, the seeding operation improves the temporal coherence and the profile of FEL pulse [14].

Scanning the probing fields over  $\tau$  yields  $w(p; \tau)$  as shown in Fig. 2. Panels (a) and (b) show the spectrograms before and after applying the streaking THz field, respectively. As the kinetic energy of the photoelectron from the  $i$ th state is  $\omega_{\text{XUV}} - I_p^{(i)}$ , the spectral peaks at  $p_{gg} = 1.73$  a.u. and  $p_{ee} = 1.94$  a.u. originate from states  $|g\rangle$  and  $|e\rangle$ , respectively. The two  $\tau$ -independent peaks recover  $W_{\text{pop}}$  in Eq. (1) since the amplitudes of  $|g\rangle$  and  $|e\rangle$  are constants. With the THz field, the two peaks in panel (b) are significantly broadened, and in the intermediate region around  $p_{eg} = 1.84$  a.u. fringes are formed. Extracting  $w(p = p_{eg}; \tau)$ , as indicated by the white dashed line in Fig. 2(b), the fringes shown in Fig. 2(c) oscillate with the period 0.4 fs, corresponding to 10.2 eV between states  $|g\rangle$  and  $|e\rangle$ , in good agreement to the oscillatory pattern of coherence  $\text{Re}[\rho_{eg}(\tau)]$ . Remarkably, the THz-streaking assisted method allows for resolving the sub-femtosecond quantum beating that cannot be achieved by a 5-fs probing XUV pulse alone. On the other hand, as depicted by Eq. (2), Fig. 2(d) for  $w(p; \tau = t_0)$  also shows the oscillatory behavior with  $p$  near  $p = p_{eg}$ , in good agreement with the sum over analytically derived Gaussian peaks. The  $p$ -dependent oscillation allows for the easy reconstruction of relative phase at arbitrary time  $\tau$ . Comparing with  $\varphi_{eg}(t_0) = 0$

in (d), the distribution for  $\varphi_{eg}(t_0) = \pi/2$  presented in (e) indicates that  $\varphi_{eg}(t_0)$  can be directly mapped by the phase of oscillatory  $w(p; \tau = t_0)$  at  $p = p_{eg}$ . Note, the fringes near  $p_{eg}$  in (b) are not merely caused by the superposition of broadened peak of  $W_{\text{pop}}$  at  $p_{ee}$  and  $p_{gg}$ . According to Eq. (2), there indeed exists the inbetween peak at  $p_{eg}$  for coherence  $W_{\text{coh}}(p_{eg})$  even without THz field, but its relative intensity can be significantly enhanced by the streaking-THz field.

The simple two-level system, as shown in Fig. 2, has demonstrated that  $\rho_{ij}(\tau)$  are well embedded in the streaking-assisted  $w(p; \tau)$ . However, the method is particularly useful when complicated energy structure is involved and the ultrafast relaxation and decoherence dynamics in open quantum systems are of concern. Here, we propose a reconstruction protocol (see S.III) to extract  $\rho_{ij}(\tau)$  in an ensemble consisting of four-level atoms that interact with near-resonant pulses [Fig. 3(a)]. Since the photoionization is evaluated based on the wave function  $|\Psi_0(t')\rangle$ , the open quantum system is simulated using the method of Monte Carlo wave function (quantum jump, see S.IV) [15], which is equivalent to the Lindblad-type master equation, allowing for the description of spontaneous emission and decoherence.

The THz-free and THz-streaking measurements are shown in Fig. 3(b1) and (b2), respectively. Due to the densely spaced energy levels, the relatively weak THz field at 0.0006 a.u. (2 MV/cm) is sufficient to signify  $w(p_{e_1e_2}; \tau)$  and  $w(p_{e_2e_3}; \tau)$  for coherences between adjacent excited states. All other parameters of the probing fields are the same as used for the two-level system. Note that in Fig. 3(b2) with spectral peaks dramatically broadened by the THz field, beating patterns along  $\tau$  are all over the spectrogram, including  $w(p_{ii}; \tau)$  ( $i = g, e_1, e_2, e_3$ ) within the excited manifold. Extracting the simulated result for populations along dashed lines in Fig. 3(b2) at  $p = p_{ii}$ , these artificial oscillations are clearly seen in Fig. 3(c1). In addition, in Fig. 3(c2) for coherences, the extracted results significantly deviate from the true  $\rho_{ij}(\tau)$  ( $i \neq j$ ). All these deviations suggest additional post-process be required to obtain the correct  $\rho_{ij}(\tau)$ . Therefore, we introduce the reconstruction protocol utilizing both the THz-free and THz-streaking  $w(p; \tau)$  to effectively eliminate the contributions from surrounding peaks (see S.III). Then, after applying quantum jump correction (only slightly influences results in our situation, the details will be discussed in the subsequent work), the reconstructed  $\rho_{ij}(\tau)$  are shown in Fig. 3(d) comparing with the true  $\rho_{ij}(\tau)$ . Except for the poor agreement around  $t_0$  as resolving the fast excitation dynamics is restricted by the

relatively large XUV pulse duration, the reconstructed  $\rho_{ij}(\tau)$  from the simulated measurement well recovers the true  $\rho_{ij}(\tau)$ , validating the feasibility of density matrix reconstruction using streaking-assisted photoelectron spectra.

In summary, a spectroscopic protocol is proposed to fully describe the evolution of density matrix elements, which can be reconstructed from streaking-assisted photoelectron spectrum. With the XUV pulse of fs-scale width, the beating feature of the quantum coherence can be retrieved with the sub-fs precision, less restricted by the duration of probing field than in conventional transient spectroscopies. The analysis of the streaking process is substantially simplified by a model with the spectral distribution described by the sum over Gaussian peaks, whose characteristic momenta effectively separate all density matrix elements. The model also indicates the photoelectronic spectrum oscillates with  $p$  near the characteristic momentum  $p_{ij}$  for coherence, providing an innovative single- $\tau$  approach to phase reconstruction between quantum states at arbitrary time. Above all, the systematic protocol of  $\rho_{ij}(\tau)$ -reconstruction is demonstrated by a simulated measurement observing the excitation and decoherence dynamics in a multilevel open system. The method offers the possibility to observe the sub-femtosecond decoherence of attosecond photo-ionization in small atomic and molecular systems. For more complex systems, e.g., biological molecules and complexes, the coherent energy transfer in photosynthetic complexes may also be investigated.

The study was supported by National Natural Science Foundation of China (NSFC) (11420101003, 61675213, 11604347, 91636105), Shanghai Sailing Program (16YF1412600).

---

\* [yantm@sari.ac.cn](mailto:yantm@sari.ac.cn)

† [jiangyh@sari.ac.cn](mailto:jiangyh@sari.ac.cn)

- [1] S. Pabst, L. Greenman, P. J. Ho, D. A. Mazziotti, and R. Santra, *Phys. Rev. Lett.* **106**, 053003 (2011).
- [2] C. Arnold, O. Vendrell, and R. Santra, *Phys. Rev. A* **95**, 033425 (2017).
- [3] G. S. Engel, T. R. Calhoun, E. L. Read, T.-K. Ahn, T. Mančal, Y.-C. Cheng, R. E. Blankenship, and G. R. Fleming, *Nature* **446**, 782 (2007).
- [4] E. Collini and G. D. Scholes, *Science* **323**, 369 (2009).



- [5] E. Collini, C. Y. Wong, K. E. Wilk, P. M. G. Curmi, P. Brumer, and G. D. Scholes, *Nature* **463**, 644 (2010).
- [6] J. Yuen-Zhou, J. J. Krich, M. Mohseni, and A. Aspuru-Guzik, *Proc. Nat. Acad. Sci.* **108**, 17615 (2011).
- [7] E. Goulielmakis, Z.-H. Loh, A. Wirth, R. Santra, N. Rohringer, V. S. Yakovlev, S. Zherebtsov, T. Pfeifer, A. M. Azzeer, M. F. Kling, S. R. Leone, and F. Krausz, *Nature* **466**, 739 (2010).
- [8] C. Ott, A. Kaldun, L. Argenti, P. Raith, K. Meyer, M. Laux, Y. Zhang, A. Blättermann, S. Hagstotz, T. Ding, R. Heck, J. Madroñero, F. Martín, and T. Pfeifer, *Nature* **516**, 374 (2014).
- [9] M. Kowalewski, K. Bennett, J. R. Rouxel, and S. Mukamel, *Phys. Rev. Lett.* **117**, 043201 (2016).
- [10] W. Helml, A. R. Maier, W. Schweinberger, I. Grguraš, P. Radcliffe, G. Doumy, C. Roedig, J. Gagnon, M. Messerschmidt, S. Schorb, C. Bostedt, F. Grüner, L. F. DiMauro, D. Cubaynes, J. D. Bozek, T. Tschentscher, J. T. Costello, M. Meyer, R. Coffee, S. Düsterer, A. L. Cavalieri, and R. Kienberger, *Nature Photonics* **8**, 950 (2014).
- [11] R. Kienberger, M. Hentschel, M. Uiberacker, C. Spielmann, M. Kitzler, A. Scrinzi, M. Wieland, T. Westerwalbesloh, U. Kleineberg, U. Heinzmann, M. Drescher, and F. Krausz, *Science* **297**, 1144 (2002).
- [12] U. Fröhling, M. Wieland, M. Gensch, T. Gebert, B. Schütte, M. Krikunova, R. Kalms, F. Budzyn, O. Grimm, J. Rossbach, E. Plönjes, and M. Drescher, *Nature Photonics* **3**, 523 (2009).
- [13] I. Grguraš, A. R. Maier, C. Behrens, T. Mazza, T. J. Kelly, P. Radcliffe, S. Düsterer, A. K. Kazansky, N. M. Kabachnik, T. Tschentscher, J. T. Costello, M. Meyer, M. C. Hoffmann, H. Schlarb, and A. L. Cavalieri, *Nature Photonics* **6**, 852 (2012).
- [14] S. Ackermann, A. Azima, S. Bajt, J. Bödewadt, F. Curbis, H. Dachraoui, H. Delsim-Hashemi, M. Drescher, S. Düsterer, B. Faatz, M. Felber, J. Feldhaus, E. Hass, U. Hipp, K. Honkavaara, R. Ischebeck, S. Khan, T. Laarmann, C. Lechner, T. Maltezopoulos, V. Miltchev, M. Mittenzwey, M. Rehders, J. Rönsch-Schulenburg, J. Rossbach, H. Schlarb, S. Schreiber, L. Schroedter, M. Schulz, S. Schulz, R. Tarkeshian, M. Tischer, V. Wacker, and M. Wieland, *Phys. Rev. Lett.* **111**, 114801 (2013).
- [15] J. Dalibard, Y. Castin, and K. Mølmer, *Phys. Rev. Lett.* **68**, 580 (1992).

## Analysis of the streaking-assisted ionization

It is assumed that the atom is subject to linearly polarized fields and the momentum distribution of photoelectrons,  $w(p) = |p||M_p|^2$ , is only collected along the polarization direction. The amplitude of the direct ionization with the strong field approximation (SFA) in the length gauge reads,

$$M_p = \lim_{t \rightarrow \infty} \int^t dt' e^{iS_p(t')} \langle p + A(t') | \hat{\mu} E(t') | \Psi_0(t') \rangle \quad (3)$$

where  $S_p(t') = \frac{1}{2} \int^{t'} dt'' [p + A(t'')]^2$ . The initial state,  $|\Psi_0(t')\rangle$ , may be prepared as the superposition of states  $\{|\psi_i\rangle\}$  of the ionization energy  $I_p^{(i)}$ ,  $|\Psi_0(t')\rangle = \sum_i c_i(t') e^{iI_p^{(i)} t'} |\psi_i\rangle$ . Substituting the superposition into Eq. (3),

$$M_p = \lim_{t \rightarrow \infty} \sum_i \int^t dt' c_i(t') \mu_i[k(t')] E(t') e^{iS_{p, I_p^{(i)}}(t')}, \quad (4)$$

with  $k(t') = p + A(t')$ , the dipole matrix element  $\mu_i(k) \equiv \langle k | \hat{\mu} | \psi_i \rangle$  and the action  $S_{p, I_p^{(i)}}(t') = \int^{t'} dt'' \left[ k(t'')^2/2 + I_p^{(i)} \right]$ . Defining  $M_p^{(i)}$  the integral in Eq. (4), we recast  $M_p = \sum_i M_p^{(i)}$  a superposition of transition amplitudes from all components of initial states.

### Partial contribution from $M_p^{(i)}$

In the following we focus on the partial contribution  $M_p^{(i)}$  from the channel of initial state  $i$ . When only the XUV pulse is present,  $E(t') = E_{\text{XUV}}(t')$  and  $A(t') = A_{\text{XUV}}(t')$ . Since the amplitude  $A_0^{(\text{XUV})} = E_0^{(\text{XUV})}/\omega_{\text{XUV}}$  is relatively small as  $\omega_{\text{XUV}}$  is large, the action reduces to  $S_{p, I_p^{(i)}}(t') \simeq \int^{t'} \left[ \frac{1}{2} p^2 + I_p^{(i)} \right] dt'' = \left( \frac{1}{2} p^2 + I_p^{(i)} \right) t'$ . Defining  $E_{\text{XUV}}(t') = \mathcal{E}_{\text{XUV}}(t' - \tau) \cos[\omega_{\text{XUV}}(t' - \tau)]$  with  $\mathcal{E}_{\text{XUV}}(t' - \tau)$  the pulse envelope centered at  $\tau$ , the phase in the exponential reads  $\frac{p^2}{2} + I_p^{(i)} \pm \omega_{\text{XUV}}$ , and the fast oscillating part (the "+" term) can be neglected after the integration. Also neglecting the dipole term, the transition amplitude is approximately

$$M_p^{(i)}(\tau) \sim \lim_{t \rightarrow \infty} \frac{1}{2} e^{i\left(\frac{p^2}{2} + I_p^{(i)}\right)\tau} \int_{-\infty}^t dt' c_i(t') \mathcal{E}_{\text{XUV}}(t' - \tau) e^{i\Omega_{ii}(p)(t' - \tau)}, \quad (5)$$

where  $\Omega_{ii}(p) = p^2/2 + I_p^{(i)} - \omega_{\text{XUV}}$ . It can be viewed as the short time Fourier transform of  $c_i(t)$  with the window function  $\mathcal{E}_{\text{XUV}}(t)$ . The spectrum  $|M_p^{(i)}(\tau)|^2$  peaks at  $p^2/2 = \omega_{\text{XUV}} - I_p^{(i)}$ .

With the presence of both XUV and THz pulses, the conditions  $A_0^{(\text{XUV})} \ll A_0^{(\text{THz})}$  and  $E_0^{(\text{XUV})} > E_0^{(\text{THz})}$  justify the approximation  $k(t') \simeq p + A_{\text{THz}}(t')$ . With the center time of

the THz field  $\tau$  coincident with the XUV field,  $E_{\text{THz}}(t') = \mathcal{E}_{\text{THz}}(t' - \tau) \cos[\omega_{\text{THz}}(t' - \tau)]$ , since the duration of the XUV pulse is much smaller than the THz field, the latter is approximately linear, i.e.,  $A_{\text{THz}}(t') \simeq \alpha(t' - \tau)$ , around the streaking time when ionization events occur. Conducting the series expansion of  $A_{\text{THz}}(t')$  around  $\tau$ , it is shown that the slope  $\alpha = -E_0^{(\text{THz})}$ . Substituting the linear approximation of  $A_{\text{THz}}(t')$  into action  $S_{p,I_p}^{(i)}(t')$ , we find  $S_{p,I_p}^{(i)}(t') = \left[ \left( \frac{p^2}{2} + I_p^{(i)} \right) + \alpha p \left( \frac{t'}{2} - \tau \right) + \frac{\alpha^2}{6} (t'^2 - 3t'\tau + 3\tau^2) \right] t'$ . The quadratic term of  $\alpha$  is negligible when  $\alpha$  is small, thus  $S_{p,I_p}^{(i)}(t') \simeq \frac{\alpha p}{2} t'^2 + \left( \frac{p^2}{2} + I_p^{(i)} - \alpha p \tau \right) t' = \frac{\alpha p}{2} (t' - \tau)^2 + \left( \frac{p^2}{2} + I_p^{(i)} \right) (t' - \tau) + \phi_i(p, \tau)$  with  $\phi_i(p, \tau) = \left( \frac{p^2}{2} + I_p^{(i)} \right) \tau - \left( \frac{\alpha p}{2} \right) \tau^2$  a phase that can be factored out of the integration over  $t$ . Similar to the analysis without the THz streaking, substituting the XUV field,  $E_{\text{XUV}}(t') = \mathcal{E}_{\text{XUV}}(t' - \tau) \cos[\omega_{\text{XUV}}(t' - \tau)]$ , into  $M_p^{(i)}(\tau)$ , the transition amplitude in the polarization direction is given by

$$M_p^{(i)}(\tau) \sim \frac{1}{2} e^{i\phi_i(p, \tau)} \lim_{t \rightarrow \infty} \int_{-\infty}^t dt' c_i(t') \mathcal{E}_{\text{XUV}}(t' - \tau) e^{i \left[ \frac{\alpha p}{2} (t' - \tau)^2 + \Omega_i(p)(t' - \tau) \right]}, \quad (6)$$

as long as the XUV field is within the linear region of the THz field. Comparing with Eq. (5), the appearance of an extra quadratic term in the exponent,  $(\alpha p/2)(t' - \tau)^2$ , results in the spectral broadening.

*Gaussian envelope of  $\mathcal{E}_{\text{XUV}}$  and slowly varying envelope approximation of  $c_i(t')$*

Assuming the envelope is Gaussian,  $\mathcal{E}_{\text{XUV}}(t' - \tau) = E_0^{(\text{XUV})} e^{-(t' - \tau)^2/2\sigma^2}$ , we cast the integral part of Eq. (6) as  $I = \int_{-\infty}^{\infty} dt' c_i(t') e^{-X(t' - Y_i)^2 + C_i}$ , where  $X = b(p)/2$ ,  $Y_i = \tau + i\Omega_{ii}(p)/b(p)$ ,  $C_i = [i\Omega_{ii}(p)]^2/2b(p)$  and  $b(p) = 1/\sigma^2 - i\alpha p$ . Integrating by parts, it is shown that

$$I = \frac{\sqrt{\pi} e^{C_i}}{2\sqrt{X}} E_0^{(\text{XUV})} \left[ c_i(\tau + \Delta\tau) + c_i(\tau - \Delta\tau) - \int_{\tau - \Delta\tau}^{\tau + \Delta\tau} dt' \text{Erf} \left[ \sqrt{X}(t' - Y_i) \right] \dot{c}_i(t') \right], \quad (7)$$

where  $\text{Erf}[\cdot]$  is the error function, and  $\Delta\tau$  is an appropriate value to estimate the active temporal region of the XUV pulse. As a rule of thumb,  $\Delta\tau = 3\sigma$  is sufficient to cover the main part of the  $\mathcal{E}_{\text{XUV}}(t' - \tau)$ .

In Eq. (7), the known properties of  $c_i(t')$  may yield further simplification. If  $c_i(t')$  changes slowly in regards to  $2\Delta\tau$ ,  $\dot{c}_i(t')\Delta\tau/c_i(t') \ll 1$ , Eq. (7) becomes  $I = \frac{\sqrt{\pi} e^{C_i}}{\sqrt{X}} \bar{c}_i(\tau)$  with  $\bar{c}_i(\tau)$  the averaged wave amplitude near  $\tau$ . In other words, if the XUV pulse is sufficiently narrow, the wave amplitude  $c_i(\tau)$  can always be well resolved within the window. Then the ionization

amplitude reads

$$\begin{aligned}
M_p^{(i)}(\tau) &= \frac{E_0^{(\text{XUV})}}{2} \bar{c}_i(\tau) e^{i\phi_i(p,\tau)} \sqrt{\frac{\pi}{X}} e^{C_i} \\
&= \frac{E_0^{(\text{XUV})}}{2} \bar{c}_i(\tau) e^{i\phi_i(p,\tau)} \sqrt{\frac{2\pi}{b(p)}} e^{-\frac{\Omega_i^2(p)}{2b(p)}}
\end{aligned} \tag{8}$$

### *Ionization probability and momentum distribution*

In the following, assuming the wave function varies slowly in regards to the window width of the XUV pulse, we calculate the ionization signal by substituting Eq. (8), the partial contribution from channel  $i$ , into  $|M_p(\tau)|^2 = \left| \sum_i M_p^{(i)}(\tau) \right|^2$ ,

$$|M_p(\tau)|^2 = \frac{\pi(E_0^{(\text{XUV})})^2}{2|b(p)|} \left\{ \sum_i |c_i|^2 e^{-\frac{\Omega_i^2(p)}{|b(p)\sigma|^2}} + \sum_{i,j \neq i} (c_i^* c_j) e^{-i[\phi_i(p,\tau) - \phi_j(p,\tau)]} e^{-\frac{1}{2} \left[ \frac{\Omega_{ii}^2(p)}{b^*(p)} + \frac{\Omega_{jj}^2(p)}{b(p)} \right]} \right\}.$$

Here,  $\bar{c}_i(\tau)$  is abbreviated by  $c_i$ . The exponent in the last term that is associated to the contribution from the coherence can be further reduced. First,

$$\frac{\Omega_{ii}^2(p)}{b^*(p)} + \frac{\Omega_{jj}^2(p)}{b(p)} = \frac{\text{Re}[b(p)][\Omega_{ii}^2(p) + \Omega_{jj}^2(p)] + i\text{Im}[b(p)][\Omega_{ii}^2(p) - \Omega_{jj}^2(p)]}{|b(p)|^2}.$$

By substituting  $b(p)$  and  $\Omega_{ii}(p)$ , one can show in the above equation,  $\Omega_{ii}^2(p) + \Omega_{jj}^2(p) = 2\Omega_{ij}^2(p) + \Delta_{ij}^2/2$  and  $\Omega_{ii}^2(p) - \Omega_{jj}^2(p) = 2\Omega_{ij}^2(p)\Delta_{ij}$ , where  $\Delta_{ij} = I_p^{(i)} - I_p^{(j)}$  and  $\Omega_{ij}(p) = [\Omega_i(p) + \Omega_j(p)]/2 = p^2/2 + (I_p^{(i)} + I_p^{(j)})/2 - \omega_{\text{XUV}}$  consistent with the definition of  $\Omega_{ii}(p)$ .

Using  $\text{Re}[b(p)] = 1/\sigma^2$  and  $\text{Im}[b(p)] = -\alpha p$ , we have

$$\frac{\Omega_{ii}^2(p)}{b^*(p)} + \frac{\Omega_{jj}^2(p)}{b(p)} = \frac{2\Omega_{ij}^2(p)}{|b(p)\sigma|^2} + \frac{\Delta_{ij}^2}{2|b(p)\sigma|^2} - i \frac{2\alpha p \Omega_{ij}(p) \Delta_{ij}}{|b(p)|^2}.$$

Also note that in  $|M_p|^2$  the phase difference  $\phi_i(p,\tau) - \phi_j(p,\tau) = (I_p^{(i)} - I_p^{(j)})\tau = \Delta_{ij}\tau$ . Therefore, the analytical expression of spectral peaks, Eq. (1) and (2) in the main text, is derived,  $|M_p(\tau)|^2 = \frac{\pi(E_0^{(\text{XUV})})^2}{2|b(p)|} \{W_{\text{pop}}(p;\tau) + W_{\text{coh}}(p;\tau)\}$ , where

$$W_{\text{pop}}(p;\tau) = \sum_i \rho_{ii}(\tau) e^{-\frac{\Omega_{ii}^2(p)}{|b(p)\sigma|^2}}, \tag{9}$$

$$\begin{aligned}
W_{\text{coh}}(p;\tau) &= \sum_{i,j \neq i} \rho_{ij}(\tau) e^{-\frac{\Omega_{ij}^2(p)}{|b(p)\sigma|^2}} e^{-\frac{(\Delta_{ij}/2)^2}{|b(p)\sigma|^2}} e^{i \frac{\alpha p \Omega_{ij}(p) \Delta_{ij}}{|b(p)|^2}} \\
&= 2 \sum_{i,j < i} \text{Re} \left[ \rho_{ij}(\tau) e^{i \frac{\alpha p \Omega_{ij}(p) \Delta_{ij}}{|b(p)|^2}} \right] e^{-\frac{\Omega_{ij}^2(p)}{|b(p)\sigma|^2}} e^{-\frac{(\Delta_{ij}/2)^2}{|b(p)\sigma|^2}},
\end{aligned} \tag{10}$$

where  $\rho_{ij}(\tau) = (c_i^* c_j) e^{-i\Delta_{ij}\tau}$  are density matrix elements. Eq. (9) and (10) present several features of the photoelectronic spectrum in the streaking regime,

- The exponential  $e^{-\Omega_{ij}^2(p)/|b(p)\sigma|^2}$  in Eq. (9) and (10) indicates that both  $W_{\text{pop}}(p)$  and  $W_{\text{coh}}(p)$  share the same spectral profile of Gaussian envelope. The spectral peak is located at  $p = p_{ij}$  that satisfies  $\Omega_{ij}(p_{ij}) = 0$ , effectively mapping  $\rho_{ij} \rightarrow p_{ij}$  and separating different density matrix elements in the spectrum. Note, the momentum  $p_{ij} (i \neq j)$  for coherence is between  $p_{ii}$  and  $p_{jj}$  for corresponding populations. The width of the spectral peak is determined by  $|b(p)\sigma|^2 = 1/\sigma^2 + (\alpha p\sigma)^2$ . Without the THz pulse, the XUV pulse alone leads to the width of the spectral peak  $\sim 1/\sigma$ , which is exactly the reciprocity relation between temporal and spectral domains and complies with the uncertainty principle. With the THz pulse, the spectral width can be effectively broadened by  $\alpha$ , the amplitude of streaking-THz field.
- $W_{\text{coh}}(p; \tau)$  is typically much smaller than  $W_{\text{pop}}(p; \tau)$  due to factor  $e^{-(\Delta_{ij}/2)^2/|b(p)\sigma|^2}$ . When  $\Delta_{ij}$  is large, it is unlikely to observe the peak of  $W_{\text{coh}}(p; \tau)$  clearly. However, the extra THz field helps alleviate the reduction caused by the factor and enhance  $W_{\text{coh}}(p; \tau)$ . Therefore, the THz-streaking technique is particular useful when  $\Delta_{ij}$  is large and the coherence is of interest. On the other hand, if  $\Delta_{ij}$  is small, the coherence can have already been clearly seen even without THz field. It means, the strength of THz field should be optimized depending on the
- Although the method can be used to study the multilevel system, the resolutions in temporal and spectral domains still follow uncertainty principle dependent on the XUV pulse width  $\sigma$ , i.e., one cannot achieve high spectral resolution and temporal resolution simultaneously. As shown by Eq. (6), the time correlation between electric field  $\mathcal{E}(\tau)$  of the finite pulse width and  $c_i(\tau)$  smears the true  $c_i(\tau)$ . However, the beating patterns of  $\text{Re}[\rho_{ij}(\tau)]$  can be well temporally resolved beyond  $\sigma$ , as long as  $W_{\text{coh}}$  is measurable.
- The factor  $e^{i\frac{\alpha p \Omega_{ij}(p) \Delta_{ij}}{|b(p)|^2}}$  in (10) also suggests the momentum distribution oscillates with  $p$  around  $p_{ij}$ . Increasing the THz strength may help observe the oscillation. Besides the phase reconstruction as mentioned in the main text, the frequency of the oscillation may also be used to calibrate the light field due to the dependence on  $\alpha$  and  $\omega_{\text{XUV}}$ .

## Reconstruction of relative phase

The relative phase can be extracted from photoelectronic spectrum. Assuming that the initial phase is given by  $\varphi_i$  for the  $i$ th state,  $|\Psi_0(t)\rangle = \sum_i c_i(t) e^{i\varphi_i} e^{iI_p^{(i)}t} |i\rangle$  and  $c_i(t) \in \mathbb{R}$  is the amplitude of the wave function, the element  $\rho_{ij}$  can be represented by the relative phase embedded expression,  $\rho_{ij}(t) = (c_i(t) e^{i\varphi_i})^* (c_j(t) e^{i\varphi_j}) e^{-i\Delta_{ij}t} = |\rho_{ij}(t)| e^{-i(\varphi_i - \varphi_j)} e^{-i\Delta_{ij}t}$  with  $|\rho_{ij}(t)| = c_i(t) c_j(t)$ . Thus, the coherence part Eq. (10) reads,

$$\begin{aligned} W_{\text{coh}}(p; \tau) &= 2 \sum_{i,j < i} |\rho_{ij}(\tau)| \text{Re} \left[ (e^{-i(\varphi_i - \varphi_j)} e^{-i\Delta_{ij}\tau} e^{i \frac{\alpha p \Omega_{ij}(p) \Delta_{ij}}{|b(p)|^2}}) \right] e^{-\frac{\Omega_{ij}^2(p)}{|b(p)\sigma|^2}} e^{-\frac{(\Delta_{ij}/2)^2}{|b(p)\sigma|^2}} \\ &= 2 \sum_{i,j < i} |\rho_{ij}(\tau)| \cos \left[ \Delta_{ij} \left( \tau - \frac{\alpha p \Omega_{ij}(p)}{|b(p)|^2} \right) + \varphi_i - \varphi_j \right] e^{-\frac{\Omega_{ij}^2(p)}{|b(p)\sigma|^2}} e^{-\frac{(\Delta_{ij}/2)^2}{|b(p)\sigma|^2}} \end{aligned}$$

Since near  $p \simeq p_{ij}$ , the term  $\frac{\alpha p \Omega_{ij}(p)}{|b(p)|^2} = \frac{\alpha p \left( \frac{p^2}{2} + (I_p^{(i)} + I_p^{(j)})/2 - \omega_{XUV} \right)}{\frac{1}{\sigma^4} + \alpha^2 p^2} \simeq \frac{\alpha p_{ij}^2}{\frac{1}{\sigma^4} + \alpha^2 p_{ij}^2} (p - p_{ij})$  is approximately linear to  $p$ ,  $W_{\text{coh}}(p; \tau)$  reads

$$\begin{aligned} W_{\text{coh}}(p; \tau) &\simeq 2 \sum_{i,j < i} |\rho_{ij}(\tau)| \cos \left[ \Delta_{ij} \left( \tau - \frac{\alpha p_{ij}^2}{\frac{1}{\sigma^4} + \alpha^2 p_{ij}^2} (p - p_{ij}) \right) + \varphi_i - \varphi_j \right] e^{-\frac{\Omega_{ij}^2(p)}{|b(p)\sigma|^2}} e^{-\frac{(\Delta_{ij}/2)^2}{|b(p)\sigma|^2}} \\ &= 2 \sum_{i,j < i} |\rho_{ij}(\tau)| \cos \left[ -\frac{\Delta_{ij} \alpha p_{ij}^2}{\frac{1}{\sigma^4} + \alpha^2 p_{ij}^2} (p - p_{ij}) + \varphi_{ij}(\tau) \right] e^{-\frac{\Omega_{ij}^2(p)}{|b(p)\sigma|^2}} e^{-\frac{(\Delta_{ij}/2)^2}{|b(p)\sigma|^2}}, \end{aligned}$$

where  $\varphi_{ij}(\tau) = \Delta_{ij}\tau + (\varphi_i - \varphi_j)$  is the relative phase difference between states  $i$  and  $j$  at time  $\tau$ . Hence, the relative phase difference for arbitrary time  $\tau$  can be easily inferred from the phase of  $W_{\text{coh}}(p)$  at  $p = p_{ij}$ , when the cosine part becomes  $\cos(\varphi_{ij}(\tau))$ .

Assuming that at a given time  $\tau$ , the initial relative phase between state  $i$  and  $j$  is desired to be measured. According to the scheme in this work, one only needs to move the center of the combinational fields to time  $\tau$ , and retrieve the photoelectronic spectrum. It is expected the THz-streaking field allows one to clearly observe the oscillation around  $p = p_{ij}$ , then determine the phase at exactly this point, from which the relative quantum phase between two states can be evaluated. The advantage of the method is that it only requires a single- $\tau$  measurement for the desired time  $\tau$  without further scanning procedure over  $\tau$ .

## Protocol of $\rho_{ij}$ -reconstruction

With the information of the density matrix elements embedded in the photoelectronic momentum distribution, a systematic protocol is desired to quantitatively reconstruct the

$\rho_{ij}$ . Since the spectrum in the streaking-regime is described by model as the sum over Gaussian peaks, the components can be disentangled for the  $\rho_{ij}$ -reconstruction. The most straightforward method is to consider the twice measurements. First, with only XUV field, one is able to extract populations  $\rho_{ii}$ . Then, applying the THz field, the acquired coherence-encoded spectrum can be further processed by the known  $\rho_{ii}$  to find out the coherence  $\rho_{ij}$ . The more detailed procedure is as following,

1. With the spectrum under only the XUV field, in order to derive  $\rho_{ii}$ , read  $w(p_{ii})$  versus  $\tau$ , from which factor out the coefficient according to Eq. (9).

2. With the spectrum under both the XUV and the THz fields, for the coherence  $\rho_{ij}$ , since the signal  $w(p_{ij})$  is always positive [see, e.g., black line around  $p_{eg}$  in Fig. 2(d) in the main text] due to the contributions from adjacent Gaussian peaks  $W_{\text{pop}}(p_{ij})$  [Eq. (9)], one should subtract these background components first, then reconstruct  $\rho_{ij}$  using Eq. (10).

However, the above scheme is applicable only when energy levels are well distinguishable, i.e.,  $\rho_{ii}(\tau)$  can be clearly identified. When the energy levels are densely distributed, the THz-induced broadened spectral peaks may interfere, even between Gaussian peaks of  $W_{\text{pop}}(p)$ , leading to beating pattern of  $w(p_{ii})$  as the function of  $\tau$ , eventually yielding artificial oscillatory behavior of  $\rho_{ii}(\tau)$  after the above steps. Therefore, it is practical to first conduct the measurement without THz field, just as the conventional pump-probe experiment, to retrieve  $\rho_{ii}(\tau)$  correctly. Of course, it is required at least the XUV pulse alone is capable to resolve the energy levels. After that, introducing the THz field of appropriate intensity that enhances the coherence relevant signals  $w(p_{ij})$ , one can reconstruct  $\rho_{ij}(\tau)$  using the previously obtained  $\rho_{ii}(\tau)$ .

### Method of Monte Carlo wave function (MCWF)

In Eq. (4), the calculation of photoelectronic momentum distribution requires that the coefficients  $c_i(t)$  of all wave function are known. For an open system, however, the ensemble consisting of many samples that are different from each other has to be considered, e.g., spontaneous emission occurs randomly among atoms in an ensemble. Such problems usually requires solving the the master equation of density matrix, and the system cannot be simply described by the wave function of pure state. However, with  $\rho_s$  the density matrix of the subsystem we are interested in and  $C_m(C_m^\dagger)$  the lowering (raising) operator in the

subsystem, it has been shown the master equation with Lindblad-type relaxation operator  $\mathcal{D} = -\frac{1}{2} \sum_m (C_m^\dagger C_m \rho_s + \rho_s C_m^\dagger C_m) + \sum_m C_m \rho_s C_m^\dagger$  can be equivalently solved by the MCWF. The MCWF allows for the access to wave functions that are later used for the calculation of the photoelectronic spectrum. Further details of the MCWF may be referred to [J. Dalibard, Y. Castin, and K. Mølmer, Phys. Rev. Lett. 68, 580 (1992)].

The example in the main text shows that the four level system initially in the ground state  $|g\rangle$  is excited by the external fields, while later the transferred components in the highly excited state  $|e_2\rangle$  and  $|e_3\rangle$  may spontaneously jump back to the lowest excited state  $|e_1\rangle$ . Assuming the wave function of the system reads  $|\Psi\rangle = \sum_i c_i e^{iJ_p^{(i)}t} |i\rangle$  with the index of basis  $i \in \{g, e_1, e_2, e_3\}$ , the hamiltonian reads  $\hat{H} = \sum_i E_i |i\rangle\langle i| + \sum_{i,j} W(t) |i\rangle\langle j|$ . The off-diagonal terms,  $W(t) = 0.02e^{-(t-4100)^2/60^2} \sin(0.324t) + 0.04e^{-(t-4200)^2/60^2} \sin(0.112t)$ , describe interactions between the system with the two pulses of  $\omega_1 = 0.324$  centered at 4100 a.u., and  $\omega_2 = 0.112$  centered at 4200 a.u.. Note, because of the long pulse duration of the THz field (sin<sup>2</sup>-envelope is used in the model), the time center at 4000 a.u. is defined here as the time zero  $t_0$  for actual numerical calculation. Later for clear demonstration,  $t_0 = 4000$  a.u. will be shifted to  $t_0 = 0$  a.u. as presented in the main text. The energies of four levels are  $(E_g, E_{e_1}, E_{e_2}, E_{e_3}) = (-0.5, -0.29, -0.18, -0.06)$ . Pulse 1 [blue line in Fig. 3(a)] is near resonant with states  $|g\rangle$  and  $|e_2\rangle$ , effectively transferring population from  $|g\rangle$  to  $|e_2\rangle$ . Pulse 2 [yellow line in Fig. 3(a)] couples states within the excited manifold ( $|e_1\rangle$ - $|e_2\rangle$  and  $|e_2\rangle$ - $|e_3\rangle$ ), further distributing the population to  $|e_1\rangle$  and  $|e_3\rangle$ . Simultaneously, coherence between these states are created. Such a pulse sequence is simply to prepare dynamics for the later demonstration of the measurement, but it is not necessarily for real. The system is initially prepared in state  $|g\rangle$ .

Since in this work the relaxation channels from highly excited states  $|e_2\rangle$  or  $|e_3\rangle$  to the lowly excited state  $|e_1\rangle$  are allowed, there are certain probabilities for the wave components of  $|e_1\rangle$  and  $|e_2\rangle$  to jump back to state  $|e_1\rangle$  in each time step  $dt$ , as is considered in MCWF. The rates of the random quantum jump from states  $|e_2\rangle$  and  $|e_3\rangle$  to  $|e_1\rangle$  during the evolution of the wave function are  $\Gamma_1$  and  $\Gamma_2$ , respectively. The quantum jump occurs when  $\Gamma_i |c_i|^2 dt > \varepsilon$ , where  $\varepsilon$  is a uniformly distributed random number in the range  $[0, 1)$ . Here we set  $\Gamma_1 = \Gamma_2 = 0.007$ . Once the jump occurs, the population of the high energy state is reset to zero, while the population is transferred to the lower state, and the amplitude of the lower state is appended by a random phase. In MCWF, the single emission event is intuitively described



by the quantum jump. The single atom may experience several jump events, leading to the discontinuous "trajectories" of the wave amplitudes. From the view of a single atom, once the jump occurs at  $t_j$ ,  $c_i$  is no longer continuous. From the view of the ensemble, the jumping instants  $t_j$  vary from atom to atom, leading to diversified discontinuous trajectories.

For the  $s$ th single atom, we assume that  $c_i^{(s)}$  is the wave function generated using the MCWF method. Substituting  $c_i^{(s)}(t)$  (trajectories) into Eq. (4), the amplitude  $M_p^{(s)}$  can be calculated. The partial momentum distribution contributed from sample  $s$  is given by  $w^{(s)}(p; \tau) = |p| |M_p^{(s)}|^2$ . The observable of an open system is the statistical average over all single trajectories. Thus, the final momentum distribution is the incoherent summation over partial spectra, i.e.,  $w(p; \tau) = \sum_s w^{(s)}(p; \tau)$ . In practice, as shown in this work, 100 trajectories (time-variant  $c_i(t)$ ) are generated and stored in an ensemble, from which we later calculate the partial momentum distributions  $w^{(s)}(p; \tau)$ , and eventually obtain the final momentum distribution  $w(p; \tau)$ . The true values of the density matrix elements are also evaluated using the stored  $c_i^{(s)}$ . The population  $\rho_{ii} = \sum_s |c_i^{(s)}|^2$  and coherence  $\rho_{ij} = \sum_s (c_i^{(s)})^* c_j^{(s)}$ , as the benchmark, are compared with the reconstructed values in the main text.

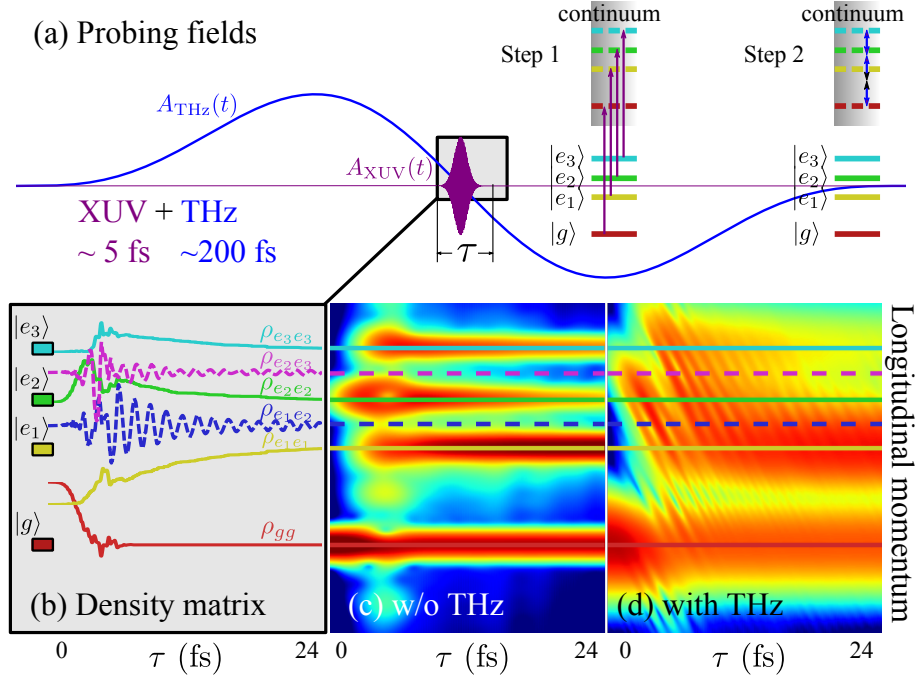


Figure 1. Schematic of the THz streaking-assisted photo-ionization experiment that allows for the real-time density matrix imaging. (a) The probing pulse configuration in the measurement. To observe the unknown quantum dynamics of an open quantum system within the temporal window (gray box), a femtosecond XUV pulse (purple) with a well-synchronized THz streaking pulse (blue) as a probe beam scans over time delay  $\tau$ . The XUV pulse is locked at the zero-crossing of the THz vector potential. (b) The energy levels and the time evolution of the density matrix elements  $\rho_{ij}$  within the time window. (c) Photoelectron momentum distribution without THz field. Populations  $\rho_{ii}$  are mapped into spectral peaks of different longitudinal momentum  $p$ , as indicated by colors of solid lines. The  $\tau$ -dependent spectral yields, labeled by red, yellow, green and cyan lines for  $\rho_{gg}$ ,  $\rho_{e_1e_1}$ ,  $\rho_{e_2e_2}$  and  $\rho_{e_3e_3}$ , respectively, reveal the evolution of populations. (d) Photoelectron momentum distribution with THz streaking. Spectral peaks are broadened and the emergent oscillating fringes, labeled along blue and purple dashed lines, can be shown to account for coherences  $\rho_{e_1e_2}$  and  $\rho_{e_2e_3}$ , respectively. The fringe can be well resolved, though the duration of the probing XUV pulse is much longer than its period of oscillation. The effective separation of  $\rho_{ij}$  along  $p$  and the temporally resolved coherence dynamics allow one to reconstruct the time evolution of  $\rho_{ij}$ .

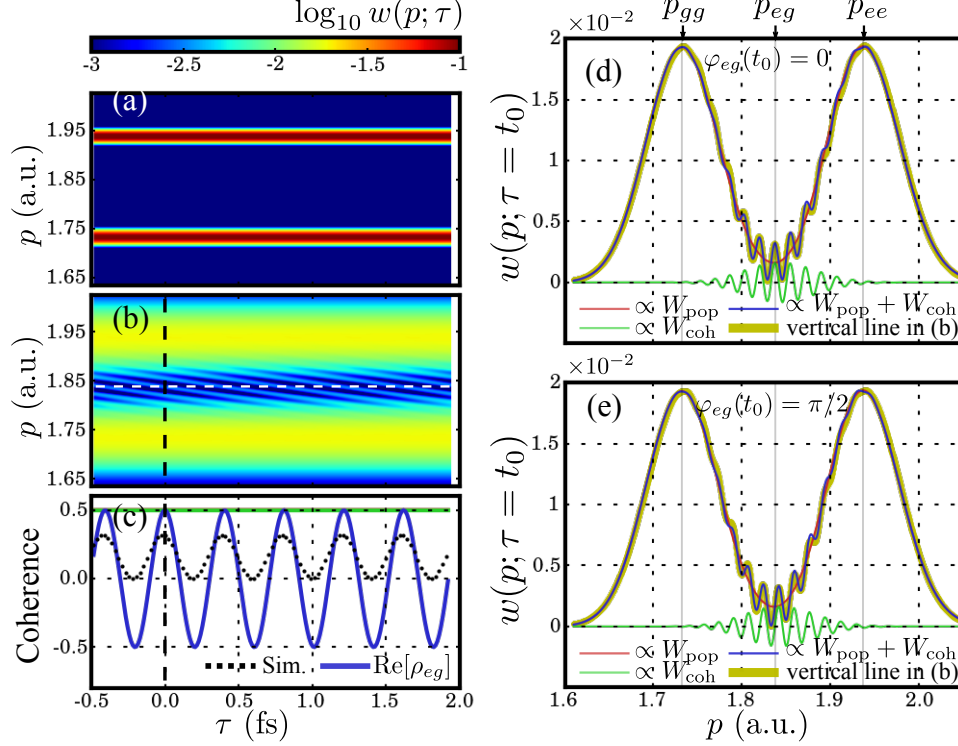


Figure 2. The temporally resolved quantum coherence with streaking-assisted photo-ionization. In a two-level system, we assume the amplitudes of the two states are constant with initial relative phase  $\varphi_{eg}(t_0) = \varphi_e - \varphi_g = 0$  at  $t_0 = 0$  fs. Panels (a) and (b) show  $w(p; \tau)$  without and with THz-streaking, respectively. Panel (c) shows both the coherence  $\text{Re}[\rho_{eg}(\tau)]$  (blue) and the temporal profile of the simulated spectral signal  $w(p = p_{eg}; \tau)$  (black dotted line), as extracted along the white dashed line in (b). Panel (d) presents  $w(p; \tau = t_0)$  as extracted along the black dashed line in (b). The extracted result (yellow) and the sum over model-based Gaussian peaks (blue), including the contributions from  $W_{\text{pop}}$  in Eq. (1) (red) and  $W_{\text{coh}}$  in Eq. (2) (green), are compared. The relative phase  $\varphi_{eg}(t_0)$  can be reconstructed with a single- $\tau$  measurement at time  $\tau = t_0$  simply by examining  $w(p; t_0)$  along the  $p$ -axis. When  $\varphi_{eg}(t_0) = 0$ , the coherence (green) at  $p = p_{eg}$  is maximized as  $\cos(\varphi_{eg}(t_0)) = 1$ . By comparison, assuming  $\varphi_{eg}(t_0) = \pi/2$ , the distribution is shown in (e), where the coherence at  $p = p_{eg}$  becomes 0.

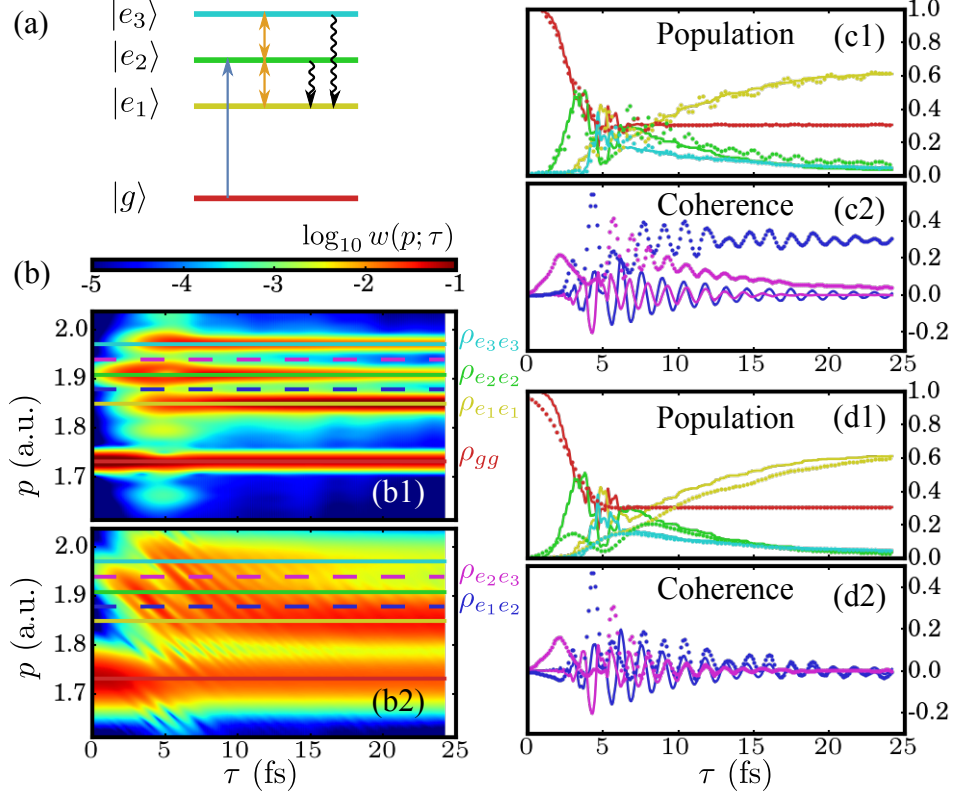


Figure 3. Reconstruction of  $\rho_{ij}(\tau)$  in a multilevel open system. The four-level system under the excitation of two-color fields is shown in (a) with energies  $(E_g, E_{e_1}, E_{e_2}, E_{e_3}) = (-0.5, -0.29, -0.18, -0.06)$  a.u.. With the two-color pulse sequence, coherences between these states are created. The relaxation processes are assumed to occur within the excited manifold, where the population in  $|e_2\rangle$  and  $|e_3\rangle$  may jump randomly to the lowest excited state  $|e_1\rangle$  with constant rates. Panels (b1) and (b2) show the photoelectron momentum distributions without and with streaking-THz field, respectively. The peaks of characteristic momenta  $p_{ij}$ , along which the results are extracted for  $\rho_{ij}$ -reconstruction, are indicated by dashed lines of the same color code as used for energy levels in (a). In (c), the THz-streaking signals extracted from (b2) (dotted lines with the same color code) are compared with the true  $\rho_{ij}$  (solid lines). Panel (d) shows the  $\rho_{ij}(\tau)$  reconstructed with the protocol.